BNL-221931-2021-JAAM

Membrane-Confined Iron Oxychloride Nanocatalysts for Highly Efficient Heterogeneous Fenton Water Treatment

S. Zhang, E. Stavitski

To be published in "ENVIRONMENTAL SCIENCE & TECHNOLOGY"

July 2021

Photon Sciences

Brookhaven National Laboratory

U.S. Department of Energy

USDOE Office of Science (SC), Basic Energy Sciences (BES) (SC-22)

DISCLAIMER

Membrane-Confined Iron Oxychloride Nanocatalysts for Highly Efficient Heterogeneous Fenton Water Treatment

Shuo Zhang,[†] Tayler Hedtke,[†] Qianhong Zhu,[†] Meng Sun,[†] Seunghyun Weon,[†,‡] Yumeng Zhao,[†,#] Eli Stavitski,[§] Menachem Elimelech,[†] Jae-Hong Kim*[,†]

[†]Department of Chemical and Environmental Engineering, Yale University, 17 Hillhouse Ave, New Haven, Connecticut 06511, United States

[‡]School of Health and Environmental Science, Korea University, Seoul 02841, Republic of Korea

[#]State Key Laboratory of Urban Water Resource and Environment, Harbin Institute of Technology, Harbin 150090, China

[§]National Synchrotron Light Source II, Brookhaven National Laboratory, Upton, New York 11973, United States

Abstract. Heterogeneous advanced oxidation processes (AOPs) allow for the destruction of aqueous organic pollutants via oxidation by hydroxyl radicals (•OH). However, practical treatment scenarios suffer from the low availability of short-lived •OH in aqueous bulk, due to both mass transfer limitations and quenching by water constituents such as natural organic matter (NOM). Herein, we overcome these challenges by loading iron oxychloride catalyst within the pores of a ceramic ultrafiltration membrane, resulting in an internal heterogeneous Fenton reaction that can degrade organics in complex water matrices with pH up to 6.2. With •OHs confined inside the nanopores (~ 20 nm), this membrane reactor completely removed various organic pollutants with water fluxes of up to 100 L m^{-2} h^{-1} (equivalent to a retention time of 10 s). This membrane, with a pore size that excludes NOM (> 300 kDa), selectively exposed smaller organics to •OH within the pores under confinement and showed excellent resiliency to representative water matrices (simulated surface water and sand filtration effluent samples). Moreover, the membrane exhibited a sustained AOPs (> 24 hours) and could be regenerated for multiple cycles. Our results suggest the feasibility of exploiting ultrafiltration membrane based AOPs platforms for organic pollutant degradation in complex water scenarios.

Keywords: membrane reactor, iron oxychloride, hydroxyl radicals, kinetics, confinement effect

Synopsis

A ceramic ultrafiltration membrane loaded with iron oxychloride nanocatalyst achieves highly efficient flow-through treatment of organic pollutants in complex water matrix due to size exclusion and nanoconfinement effect.

■ INTRODUCTION

Anthropogenic organic pollutants released into surface and ground waters pose a significant threat to the environment and human health.[1] Advanced oxidation processes (AOPs) are widely used to destroy organic pollutants, typically as a polishing step in water and wastewater treatment. The Fenton reaction is frequently employed in industrial wastewater treatment to achieve oxidative organic destruction by producing hydroxyl radicals (•OH) through the activation of hydrogen peroxide (H_2O_2).[2] Compared to the benchmark homogeneous process, which employs dissolved iron as an activation catalyst, the Fenton reaction utilizing heterogeneous catalysts offers simple operation, low cost, negligible energy input, and absence of sludge generation. Therefore, heterogeneous Fenton reaction is increasingly being considered as an alternative to the benchmark UV/H_2O_2 process used in water treatment. Nevertheless, heterogeneous AOPs remain mostly in the lab-scale developmental phase due to the relatively slow kinetics compared to their homogeneous counterparts. The extremely short lifetime of •OH in the aqueous phase (<10 μs)[3] limits its mass transfer from the site of generation (*i.e.*, catalyst surface) to the aqueous bulk, which severely restricts the radical availability.[4, 5] Furthermore, coexisting natural organic matter (NOM) in surface waters (0.1-20 mg L^{-1})[6] can block the catalytic sites and quench •OH ($k_{\cdot OH/NOM} \approx 10^9$-$10^{10}$ s^{-1})[7], which can deactivate heterogeneous catalysts and even nullify AOPs treatments targeting organic micropollutants.[8]

We propose to overcome these challenges by loading heterogeneous Fenton catalysts inside an ultrafiltration (UF) membrane porous structure and conducting the AOPs within the membrane channels. We target UF because of its low energy consumption and greater water production rate compared to membranes with smaller pores such as reverse osmosis and nanofiltration. AOPs are also most beneficial to existing water treatment processes that employ UF and conventional media filters and therefore require additional steps to remove small organics. The proposed configuration blocks organic macromolecules larger than the membrane pores from reaching the catalyst sites. Therefore, catalyst fouling and radical quenching are expected to be significantly reduced. Micropollutants smaller than the membrane pores can enter the internal porous structure or channels and be degraded by the •OH generated through surface catalysis. This unique confinement of the reaction within the membrane pores renders AOPs to be 'selective', in contrast to its hallmark property of being a non-selective treatment due to the non-selective reactivity of •OH. Past efforts in combining AOPs with membrane filtration mostly focused on reducing membrane fouling by loading catalysts on the membrane surface[9, 10] or coupling with electrocatalysis.[11, 12]

We here report a high-performance ceramic UF membrane loaded with heterogeneous Fenton catalysts for the effective removal of organic pollutants in complex water matrices. We select iron oxychloride (FeOCl) among various iron-based catalysts reported so far based on its high efficiency for H_2O_2 activation at pH up to 6.2.[13] This design marks an important contrast to some past studies that explored loading of Fenton-like catalysts onto the membrane matrix which function only at extremely low pH (< 3), the well-known hurdle in Fenton-like catalysis.[14, 15] The FeOCl-loaded ZrO_2/TiO_2 ceramic membrane (FeOCl-CM), synthesized here for the first time, demonstrates a near-complete destruction of select organic pollutants through single-pass treatment at a permeate water flux equivalent to common UF processes, with the AOPs confined within the membrane pores. This is accompanied by size exclusion of the majority of background organics larger than a molecular weight cut-off (MWCO) of 300 kDa. We further show that the membrane maintains its performance for over 24 hours and has excellent resiliency to complex water matrices containing NOM and inorganic constituents. The findings of this work highlight the practical significance of engineering membrane-confined AOPs treatment systems to deal with contaminated waters.

■ EXPERIMENTAL

Materials and Reagents. For iron-based nanocatalyst synthesis, the chemicals used are ferric chloride hexahydrate ($FeCl_3 \cdot 6H_2O$, reagent grade, > 98.0%), ferrous chloride tetrahydrate ($FeCl_2 \cdot 4H_2O$, Puriss p.a., ≥99.0%), ferrous sulfate heptahydrate ($FeSO_4 \cdot 7H_2O$, Reagentplus, ≥99.0%), copper (II) nitrate trihydrate ($Cu(NO_3)_2 \cdot 3H_2O$, Puriss p.a., 99-104%), urea (Reagentplus, ≥99.5%), polyvinylpyrrolidone (PVP, average molecular weight: 40, 000), disodium ethylenediaminetetraacetic dihydrate (EDTA-Na, 99.0-101.0% titration), ethylene glycol (anhydrous, ≥99.8%), and sodium citrate (A.C.S. reagent, supplied by Avantor Performance Materials, Inc.). For model contaminants, the chemicals used are para-chlorobenzoic acid (*p*CBA, analytical standard), bisphenol A (BPA, ≥99.0%), 2,4-dichlorophenol (DCP, > 99%), sulfamethoxazole (SMX, analytical standard), 17α-ethinylestradiol (EE, ≥98%), and atrazine (ATZ, analytical standard). For the MWCO test, the polyethylene oxide chemicals used include average molecular weights of 100, 200, 300, 400, and 600 kDa. Unless otherwise specified, all the chemicals were purchased from Sigma-Aldrich (USA) and used as received without further purification. The Suwannee River NOM was purchased from the International Humic Substances Society (USA).

Synthesis of FeOCl-CM. A circular disc-shaped ceramic UF membrane (termed as "CM"; MWCO = 400 kDa; diameter = 4.7 cm; thickness = 0.25 cm; composition, ZrO_2 and TiO_2),

purchased from Sterlitech corporation (USA) was used as the substrate. The internal growth of FeOCl platelet nanocatalysts was realized via successive incubation and annealing treatment. First, iron(III) chloride hexahydrate was dissolved in anhydrous ethanol at a concentration of 1.2 g mL^{-1}. Then, the ceramic membrane was immersed in this solution, and the whole system was sonicated for 5 h at 40 kHz and subsequently shaken for 17 hours at 160 rpm to ensure a thorough liquid impregnation. Afterwards, the membrane was removed from the iron chloride solution, held by polished silicon wafers on both sides, and then heated in air at 220°C for 1 hour with a temperature ramp rate of 10°C min^{-1}. After naturally cooled to room temperature, the material was washed with ethanol and deionized water for several times to completely remove residual impurities, and then placed in a vacuum oven for 12 hours at 40 °C. The as-prepared composite membrane was labeled as "FeOCl-CM" with the MWCO reduced to 300 kDa (Text S1 for details).

Material Characterization. Cross-sectional membrane morphologies were examined by a Hitachi SU-70 analytical field emission SEM microscope (accelerating voltage = 5 kV). X-ray diffraction (XRD) patterns were obtained using a Rigaku SmartLab X-ray Diffractometer with Cu Kα monochromatic radiation at 40 kV and 44 mA. Element mapping was captured by energy dispersive spectroscopy (EDS) coupled with a cold field emission scanning electron microscope (Hitachi SU8230). X-ray absorption spectroscopy (XAS) spectra were collected on a Beamline 8-ID (ISS) of the National Synchrotron Light Source II (Brookhaven National Laboratory, USA), using a Si (111) double crystal monochromator and a passivated implanted planar silicon detector. The data were collected at room temperature, with energy calibrated by a Fe foil, and were processed using Demter XAS analysis software. The nitrogen adsorption-desorption isotherms at -196.15 °C were detected by Autosorb-iQ-C (Quantachrome, USA), and the specific surface areas were calculated based on the multipoint Brunauer-Emmett-Teller model.

Membrane Performance Test. Flow-through catalytic reactions were conducted using a dead-end membrane test system (Figure S1). In a typical experiment, the catalytic membrane was first fixed inside the reaction module and sealed tightly by O-ring rubber bands to avoid water leakage. Then, the stock solution in a water tank, *i.e.*, the background water containing H_2O_2 (2 mM) and a model organic compound (*e.g.*, BPA, 20-50 μM), was fed into the membrane module at prescribed flow rates under different transmembrane pressures controlled by a nitrogen tank. For the long-term performance test, the stock solution was replenished every 24 hours, and no more than 5% of the spiked BPA was oxidized by H_2O_2 without catalyst present during each 24-hour interval. The membrane water fluxes were determined by a weighing balance recording online by RS-232 interface (EBTRIS2202-1S, Sartorius, Elk Grove, IL). After the membrane reaction, the permeate

sample was collected and immediately analyzed for model organic degradation, TOC removal, and iron and chloride leaching. All the experiments were performed at room temperature.

■ RESULTS AND DISCUSSION

Selection of FeOCl. Various iron-based heterogeneous catalysts have been developed to enable the Haber-Weiss cycle (*i.e.*, repeating redox reactions involving dissolved Fe(II) and Fe(III) for H_2O_2 activation and •OH generation)[2] on their solid surfaces. However, iron atoms exhibit different redox potentials and binding behaviors with H_2O_2 depending on their coordination environment. Consequently, the efficiency of an iron catalytic center for •OH production and even the tendency of undesired iron dissolution during the redox reaction can vary greatly. We first synthesized the prevailing iron-based Fenton catalysts documented so far, including α-Fe_2O_3,[16] Fe_3O_4,[17] α-FeOOH,[18] γ-FeOOH,[19] $FeCO_3$,[20] $CuFe_2O_4$,[21] and FeOCl (Text S2 and Figure S2).[22] We then compared their AOP performances when suspended in water containing 2 mM H_2O_2 at varying solution pH (Text S3). *p*CBA was employed as a probe, which reacts rapidly with •OH ($k_{\cdot OH/pCBA} \approx 5 \times 10^9$ M^{-1} s^{-1})[23] while being inert toward H_2O_2 (Figure S3). All the *p*CBA degradation rates (Figure S4) followed pseudo-first order kinetics (R^2 = 0.976-0.998), and relevant rate constants are shown in Figure 1a. Within the pH window of 3.2 to 7.0, FeOCl exhibited much higher rate constants than those of the other catalysts, with the order of FeOCl > $FeCO_3$ > $CuFe_2O_4$ > γ-FeOOH > Fe_3O_4 > α-FeOOH > α-Fe_2O_3. All catalysts, except FeOCl, suffered low performance when the solution pH surpassed 4.2. Above pH 6.2, all the other catalysts were completely deactivated, while FeOCl retained its reactivity. Our earlier study showed that FeOCl is even less sensitive to the solution pH when we shortened the reaction time to 1 minute, with a fast organics degradation at pH 7.0.[24]

FeOCl is known to function as a catalyst through the redox cycle shown in Figure 1b.[24] The outstanding catalytic property of FeOCl has been related to the fact that Fe(III) reduction to Fe(II) occurs more favorably than in other catalysts. Note that the Fe(III)-to-Fe(II) reduction is much slower than Fe(II)-to-Fe(III) oxidation, making it the rate limiting step of the redox cycle, especially at high pH for both homogeneous and heterogeneous Fenton reactions.[25] For other iron-based catalysts, various strategies, including applying external potential (*i.e.*, electro-Fenton) and providing an auxiliary reductive pathway, have been explored to enhance Fe(III) reduction on the surface.[26, 27] For FeOCl, the H_2O_2 dehydrogenation step that leads to Fe(III) reduction is known to be much more energetically favorable; *e.g.*, a first principle study[28] suggests that the H_2O_2 dehydrogenation energy barrier for FeOCl (0.23 eV) is much lower than that for Fe_2O_3 (0.76 eV), a Fenton-like catalyst frequently employed in past works.[16, 29, 30] The unique electronic property of

Fe(III) in FeOCl leading to more favorable reduction has also been noticed in other fields of application.[31, 32] As examples, significant charge transfer occurred between an intercalated polyaniline compound in FeOCl host, causing up to 25% of Fe(III) reduced to Fe(II),[31] as well as a partial Fe(III)-to-Fe(II) reduction occurring when N-methyl-2-pyrrolidinone molecules were intercalated into FeOCl layers.[32] These results, supported by mechanisms proven in the literature, demonstrated FeOCl's outstanding catalytic ability and pH adaptability, which motivated our further study to incorporate FeOCl into membrane scaffolds for heterogeneous Fenton reaction.

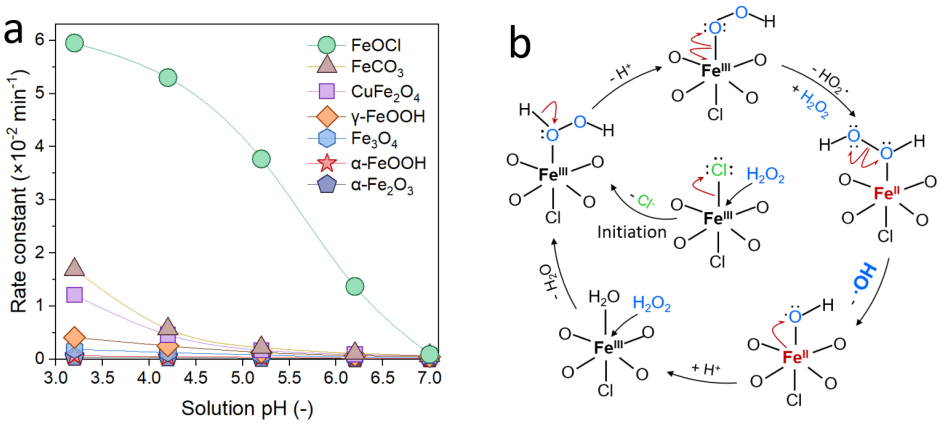

Figure 1. (a) Pseudo-first-order rate constant versus solution pH for the heterogeneous Fenton oxidation of *p*CBA in a batch reactor with different iron-based catalysts. Conditions: catalyst loading, 0.1 g L^{-1}; initial *p*CBA concentration, 20 μM; initial H_2O_2 concentration, 2 mM. (b) Proposed mechanism for FeOCl-mediated activation of H_2O_2 with •OH production.

Fabrication and Characterization of Membrane Reactor. The color of the ceramic membrane changed from white to brownish yellow after FeOCl was loaded (Figure 2a). A cross-sectional SEM view showed the random distribution of platelet nanostructures inside the membrane scaffold (Figure 2b and inset I), in clear contrast to the bare ceramic membrane (inset II). XRD diffractogram (Figure 2c) shows the characteristic FeOCl crystallographic structure with (010), (110), (021), and (040) facets at 2θ values of 11.15°, 26.1° 35.37°, and 45.81°, respectively. The dominant facet (010) indicates the stacked structure of the FeOCl layers with the interplanar spacing of about 7.92 Å according to Bragg's law. The other peaks represent the composition of the ZrO_2 and TiO_2 that constitute the ceramic membrane (Figure 2c inset).

EDS mapping (Figure 2d) on iron and chloride elements matches well with the profile of the randomly distributed nanoplatelets. According to the white line intensity in normalized near-

edge X-ray absorption spectroscopy (XANES, Figure 2e), the first derivative change of Fe K-edge spectra for FeOCl appears at 7123.4 eV, in a position between that of Fe_3O_4 (7122.9 eV) and Fe_2O_3 (7124.2 eV), suggesting the presence of both Fe(III) and Fe(II). Fourier transformed extended X-ray adsorption fine structure spectroscopy (EXAFS, Figure 2f) suggests the presence of Fe-O and Fe–Fe bonds in the planar structure, similar to those in Fe_3O_4 or Fe_2O_3. Notably, the peak at 2.20 Å evidences the out-of-plane weakly bonded Fe-Cl coordination shell (one Fe atom coordinates with two Cl atoms). These unsaturated Fe-sites have been proposed as the dominant catalytic center, leading to the outstanding catalytic performance of FeOCl compared to other iron-based catalysts.[24] Our synthesis method significantly expanded the surface area of the limited inner space of this membrane reactor. Specifically, with a FeOCl loading of 0.21 g and a specific surface area of 15.46 m^2 g^{-1} (Figure S5) the ratio of the available catalyst surface to the inner volume of FeOCl-CM (0.35 cm^3) was estimated to be 9.3×10^6 m^2 m^{-3} (Text S4).

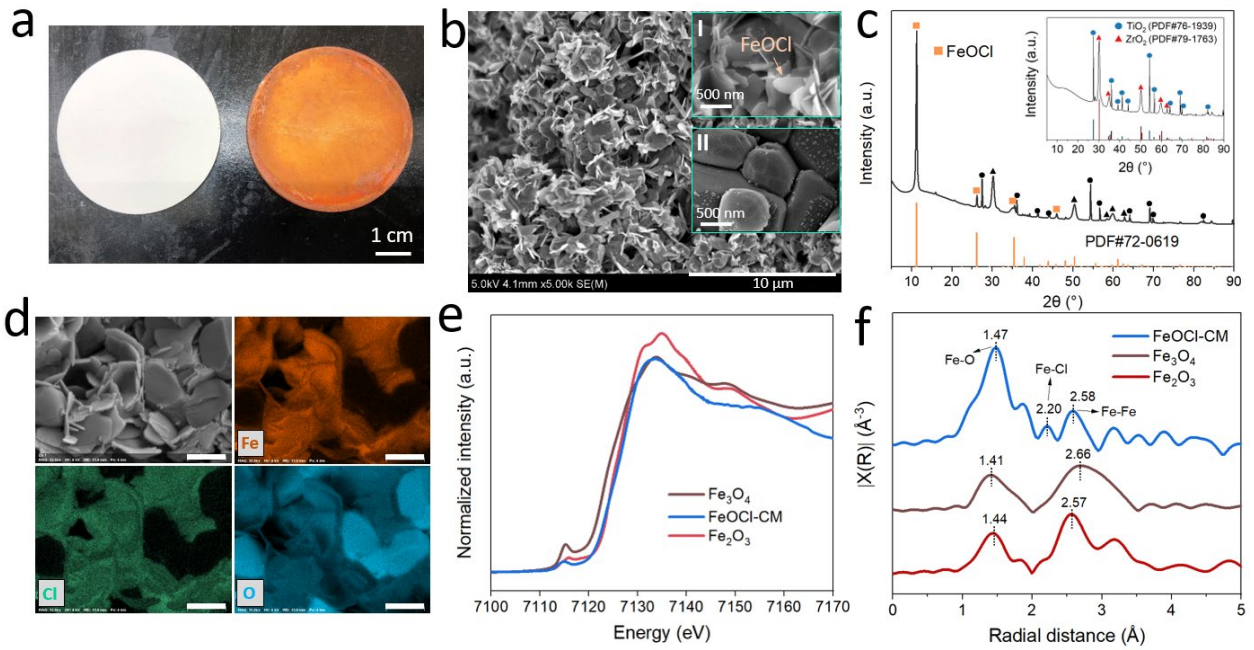

Figure 2. (a) Photographs of bare ceramic membrane (left) and FeOCl-CM composite membrane (right). (b) Cross-sectional SEM images of FeOCl-CM membrane with 5,000 times of magnification (inset figure with 25,000 times of magnification). (c) XRD pattern of FeOCl-CM membrane (peaks indicated by black circles and triangles are assigned to titanium dioxide and zirconium dioxide, respectively, as shown in the inset figure). (d) EDS mapping of the cross-sectional view of FeOCl-CM (Scale bar: 700 nm). (e) Fe K-edge XANES spectra of FeOCl-CM, Fe_3O_4, and Fe_2O_3, respectively. (f) Fourier transforms of the $\chi(k)\cdot k^3$ into R space in the range from 0 to 5 Å for FeOCl-CM, Fe_3O_4, and Fe_2O_3, respectively.

Membrane Reactivity. The catalytic Fenton reactivity was evaluated by filtering a synthetic feed water at pH 6.2 containing *p*CBA and H_2O_2 (2 mM) through the membrane samples; *i.e.*, a single

pass through the membrane. Control experiments performed using a bare CM membrane confirmed no catalytic activity in the absence of FeOCl (Figures 3a and 3b). Using as-synthesized FeOCl-CM, however, we observed a complete removal of *p*CBA at membrane water fluxes up to 100 L m^{-2} h^{-1} (LMH) (Figure 3a). This translates to the complete probe destruction at a retention time down to about 10 s within the membrane pores (see Figure S6 the correlation between transmembrane pressure, water flux, and retention time). The FeOCl-CM outperforms previously reported membrane-based Fenton-like reaction systems (Table S1) that work only either at much lower water fluxes (< 20 LMH, removal rate > 80%),[33, 34] under very acidic conditions (*e.g.*, pH ≈ 3),[35] or with extra energy assistance (*e.g.*, photo-Fenton,[36] electro-Fenton[26]).

The performance of FeOCl-CM over 5 hours of operation at steady-state water flux of 100 LMH is shown in Figure 3b. Without H_2O_2, there was a partial removal of *p*CBA due to adsorption at the initial few minutes. Such effect quickly disappeared within the first 30 min due to saturation of the adsorption sites. With the addition of H_2O_2 as the radical precursor, nearly 100% organic removal was maintained for the duration of experiments without deactivation. The results of EPR analysis (Figure 3c) performed using 5,5-dimethyl-pyrroline-oxide (DMPO) as a spin trapping agent ($k_{\cdot OH/DMPO} \approx 3.4\times10^9$ M^{-1} s^{-1})[37] confirmed $^{\bullet}OH$ as the main reactive species. The EPR signals in the permeate of FeOCl-CM was much stronger than those obtained from the batch reaction (Figure S7) performed using a high concentration of FeOCl catalyst suspension (5 g L^{-1}). The results collectively indicate that an efficient heterogeneous Fenton process driven by FeOCl occurred inside the FeOCl-CM.

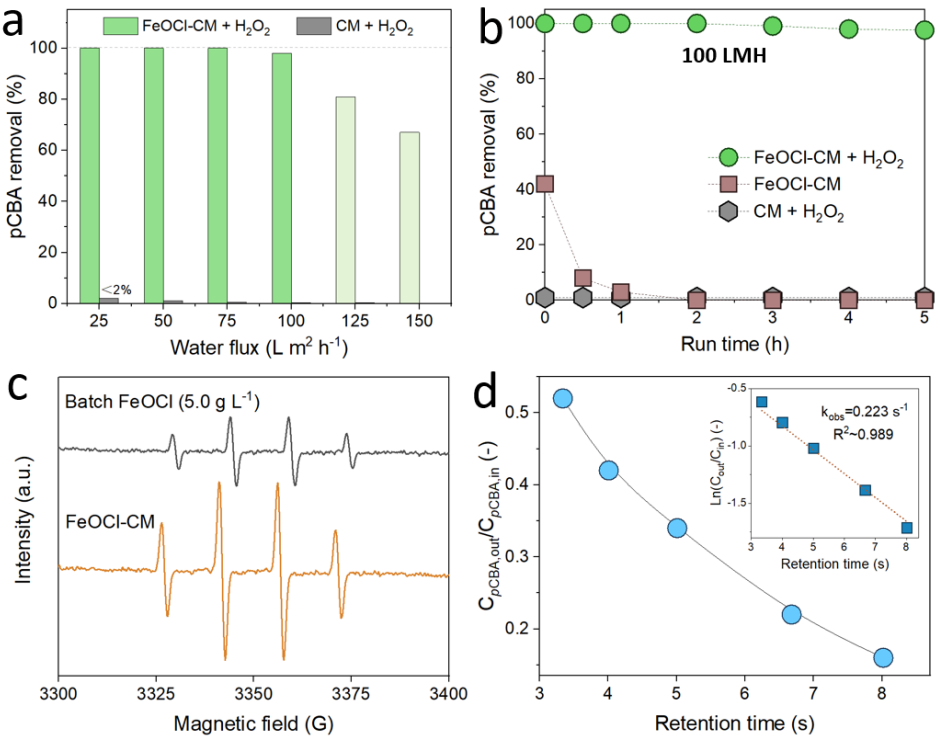

Figure 3. (a) The removal of *p*CBA as a model organic contaminant versus water flux using bare CM and FeOCl-CM as membrane reactors, respectively. The permeate samples were collected after 4-hour runtime. (b) A long-term run of FeOCl-CM for the removal of *p*CBA with (heterogeneous Fenton reaction) and without H_2O_2 (plain adsorption), respectively. (c) EPR spectra of the DMPO spin-trapping for the flow-through catalytic Fenton in FeOCl-CM and batch-mode catalytic Fenton with FeOCl nanoplates, respectively. Conditions: DMPO concentration, 0.1 mM; solution pH, 6.2; FeOCl in batch-mode: 1 g L^{-1}; water flux for FeOCl-CM: 100 LMH. The peaks emerged are DMPO−OH (a_N = a_H = 14.9 G). (d) Normalized concentration of *p*CBA versus retention time. Inset figure is the kinetics determined by linear regression analysis. The sample for outlet *p*CBA concentration was obtained after 4-hour runtime to prevent adsorption from impacting the kinetic analysis. The retention times, *i.e.*, 3.3, 4.1, 5.0, 6.7, and 8.0 s, correspond to water fluxes of 300, 250, 200, 150, and 125 LMH, respectively. Conditions of feed water for all the membrane tests: *p*CBA, 50 μM; H_2O_2, 2 mM; solution pH, 6.2.

The probe concentration profile as a function of retention time is shown in Figure 3d. Note that further increasing the permeation flux means decreasing the retention time within the membrane pores, which is conceptually equivalent to shortening the reaction time in a batch reactor. The first-order rate constant of *p*CBA destruction by FeOCl-CM (inset Figure 3d) was 0.22 s^{-1}, approximately 1,200 times higher than that obtained from batch suspension reaction (1.8 $\times 10^{-4}$ s^{-1} at pH 6.2, Figure S4). We estimate the steady-state •OH concentration confined inside the membrane to be approximately 44.6 pM ($k_{\cdot OH/pCBA} \approx 5.0\times10^9$),[23] in stark contrast to the batch-mode counterpart (~ 0.036 pM). Such an intense •OH exposure inside the membrane was partly contributed by large surface area (~ 9.3×10^6 m^2 m^{-3}) available for catalysis (Text S4). This

is unlikely to occur in the case of batch suspension reaction where particle agglomeration limits the surface availability and thus the reactivity of the whole system.[38] Supporting this assertion is the limited enhancement of •OH EPR signal intensity in response to an increasing FeOCl concentration from 1 to 5 g L^{-1} (Figure S7).

We also attribute the enhanced kinetics to the nanoconfinement effect; *i.e.*, •OH exposure is increased by confining short-lived •OH (<10 μs)[3] in a nanoscale domain. Pore size of FeOCl-CM was estimated to be approximately 20 nm (Text S1), which is at the critical value (*e.g.*, about 25 nm) that is known to trigger the nanoconfinement effect for the surface-catalyzed reaction.[39] To verify this hypothesis, we synthesized another set of FeOCl-loaded membranes using anodized aluminum oxide (AAO) as the template. The AAO template provides accurate and uniformly distributed channels with inner diameters of 20-30 nm ($NR_{20\text{-}30}$, Figure 4a) and 200-300 nm ($NR_{200\text{-}300}$, Figure 4b), respectively. In both cases, FeOCl was immobilized on the inner surface of the membrane to prevent catalyst agglomeration during comparison of the *p*CBA degradation kinetics. We found that the effective •OH concentration confined inside $NR_{20\text{-}30}$ (25 pM, k_{obs} = 0.125 s^{-1}) was much higher than that inside $NR_{200\text{-}300}$ (6.2 pM, k_{obs} = 0.031 s^{-1}) (Figure 4c). Note that the ratio of pore surface area to pore volume was approximately the same between these two membranes (Figure S8). Consequently, there was about 4 times greater of •OH exposure solely due to the decrease in the dimension of space (*i.e.*, pores of AAO) from 200-300 nm to 20-30 nm. $NR_{200\text{-}300}$ also elevated the kinetics to a large extent compared to the batch reaction (≈160 times). Although FeOCl-CM does not have such a precise pore size as AAO, it is reasonable to assume that the similar nanoconfinement effect contributes to its much improved •OH exposure compared to FeOCl suspension.

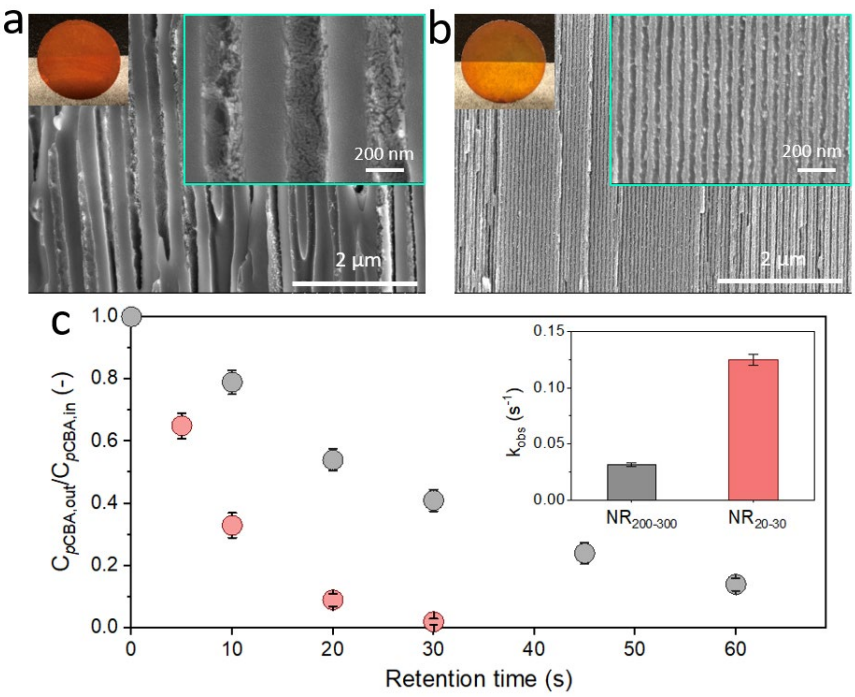

Figure 4. The cross-sectional SEM views of (a) NR_{20-30} and (b) $NR_{200-300}$, respectively. Photographs are inserted for each of them. (c) Evolution of normalized *p*CBA concentration versus retention time after catalytic treatment by the NRs. Inset figure shows the pseudo-first order kinetic constants. Error bars represent the data from triplicated tests. Conditions of entrance water: *p*CBA, 50 μM; H_2O_2, 2 mM; solution pH, 6.2.

We further tested FeOCl-CM for the removal of organic pollutants that have wide industrial, agricultural, and pharmaceutical applications, including BPA, DCP, SMX, EE, and ATZ (Figure 5). For example, BPA has been predominantly used for producing polycarbonate products, and its exposure to humans threatens the reproductive, metabolic, and neurological functions.[40, 41] We selected only small molecules that cannot be removed by typical UF membranes. Control experiments confirmed that these organics were not removed either by FeOCl-CM without H_2O_2 addition (*i.e.*, no removal by adsorption or size exclusion) or by pristine ceramic membrane with H_2O_2 addition (*i.e.*, no direct reaction with H_2O_2). When we filtered the water containing these pollutants and 2 mM H_2O_2 through FeOCl-CM, we obtained at least 92% degradation of all the model pollutants with a single pass, consistently over several hours of operation with the water flux of 100 LMH (Figure S9). The overall removal efficiency can be improved by increasing the reaction time, which is equivalent of decreasing the permeate flux. For example, by simply lowering the permeate flux to 90 LMH while keeping other conditions unchanged, we obtained the complete removal of this set of organic pollutants (Figure S10).

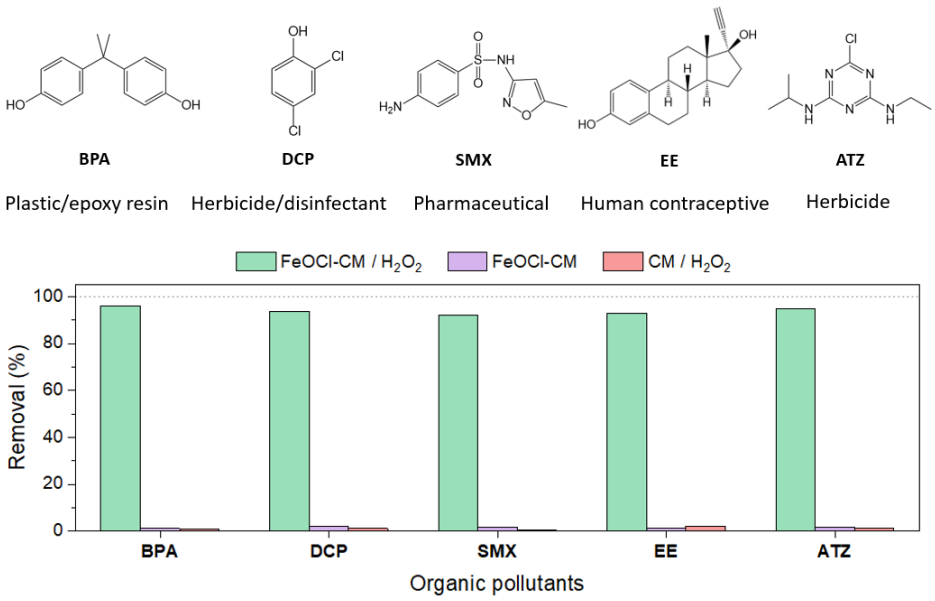

Figure 5. Removal test of five organic pollutants by membrane AOPs (*i.e.*, FeOCl-CM/H_2O_2), bare membrane adsorption (*i.e.*, FeOCl-CM), and CM substrate with H_2O_2 addition (*i.e.*, CM/H_2O_2). Conditions: organic concentration, 50 μM; H_2O_2, 2 mM; solution pH, 6.2; water flux, 100 LMH; the tested samples are after 4-hour continuous runtime.

Long Term Performance in Complex Water Matrices. FeOCl-CM maintained complete removal of BPA for at least 24 hours of continuous runtime at a water flux of 25 LMH (Figure 6a). When the run time was further prolonged to 120 hours (5 days), the catalytic activity in the membrane reactor experienced only a small loss, where over 80% of BPA removal was still achieved together with sustained consumption of H_2O_2 (Figure 6a). The loss of iron from the FeOCl basal structure was negligible of approximately 0.03 mg (Figure S11), which was far less (< 0.1%) than the total amount of iron present in the membrane (*i.e.*, 110 mg iron in the 210 mg of FeOCl that constitutes the composite membrane used in the filtration setup). However, we noticed a leaching of chloride over the duration of the experiment (Figure S11). While the release of chloride is not of any environmental concern at this concentration (~10 mg L^{-1}), we postulate that it is related to the gradual loss of catalytic activity of FeOCl over time. The Fenton-like reaction cycle in Figure 1b is initiated by the binding of H_2O_2 to Fe site that is coordinated with labile Cl ligand. The Fe is then coordinated with H_2O throughout the reaction cycle, serving as a site to coordinate with H_2O_2. The fact that the catalytic activity gradually decreases over time indicates that H_2O_2 has a higher affinity to the original Fe site bound to Cl compared to the Fe site formed after each cycle of catalysis.

We further tested FeOCl-CM with a simulated surface water containing common inorganic constituents and NOM (Table S2) spiked with BPA. NOM is known to quench •OH (second order constant of 10^9-10^{10} M^{-1} s^{-1})[7] and hinder the AOPs treatment of coexisting aromatic pollutants.[7] This effect can be seen in our batch experiment where the NOM-spiked system (5 mg L^{-1}) significantly hindered the degradation of BPA (Figure S12). However, such an interference can be largely avoided with FeOCl-CM which rejects the majority of NOM (about 70% in term of TOC) by size exclusion (Figure 6b). In other words, the FeOCl catalysts that reside inside CM pores are not exposed to the majority of NOM, allowing them to selectively target the destruction of BPA and achieve a complete removal of BPA for at least 10 hours (Figure 6c). Note that 70% NOM rejection corresponds to about 37% TOC removal for the feed solution containing both NOM (5 mg-C L^{-1}) and BPA (20 μM or 3.6 mg-C L^{-1}) (Figure 6b, middle column, without H_2O_2 addition). But the total TOC removal reached 82% due to the combined removal of large NOM by size exclusion (37%) and destruction of BPA through FeOCl catalysis (45% removal in terms of total TOC of the feed) within merely 40 seconds of retention time (25 LMH).

A fraction of NOM would enter the pore and could have contributed to catalyst deactivation. It is also known that exposure of catalysts to organic pollutants can result in deactivation due to a gradual occupation of the reactive sites.[8, 42] Such a poisoning effect was found to be minor with FeOCl within the experimental timeframe. The surface of FeOCl platelets between interlayers (d-spacing of 7.92 Å) presumably were protected from the entrance of BPA molecules with a comparable size of about 7.52 Å (van der Waals diameter; determined by a fast calculation method[43]) as well as small NOM that passes through the membrane. In contrast, H_2O_2 precursor molecules, with a much smaller size (2.5 Å mean diameter) and a high affinity to FeOCl's polarized surfaces due to the Lewis base property,[44] will likely achieve an easier intercalation into the van der Waals layers for •OH production.[45] Consequently, an additional size exclusion phenomenon (*i.e.*, in addition to size exclusion by CM membrane pores) is in a play to further protect catalysts from deactivation by organics (Figure 6d).

We also observed that most coexisting inorganic substances did not show an evident effect on the FeOCl-CM performance. However, we noticed that carbonate species tends to deactivate surface iron sites likely due to the formation of a passive layer.[46, 47] When the solution alkalinity was increased to 600 μeq L^{-1} (*i.e.*, 59.0 mg L^{-1} $CaCO_3$) at a fixed pH of 6.2, the BPA removal was maintained only for the first 4 hours (Figure 6c). It should be noted that FeOCl-CM maintained near complete BPA removal efficiency for at least 12 hours under an alkalinity of 300 μeq L^{-1} (*i.e.*, 29.5 mg L^{-1} $CaCO_3$), which is the level found in most surface waters.[48]

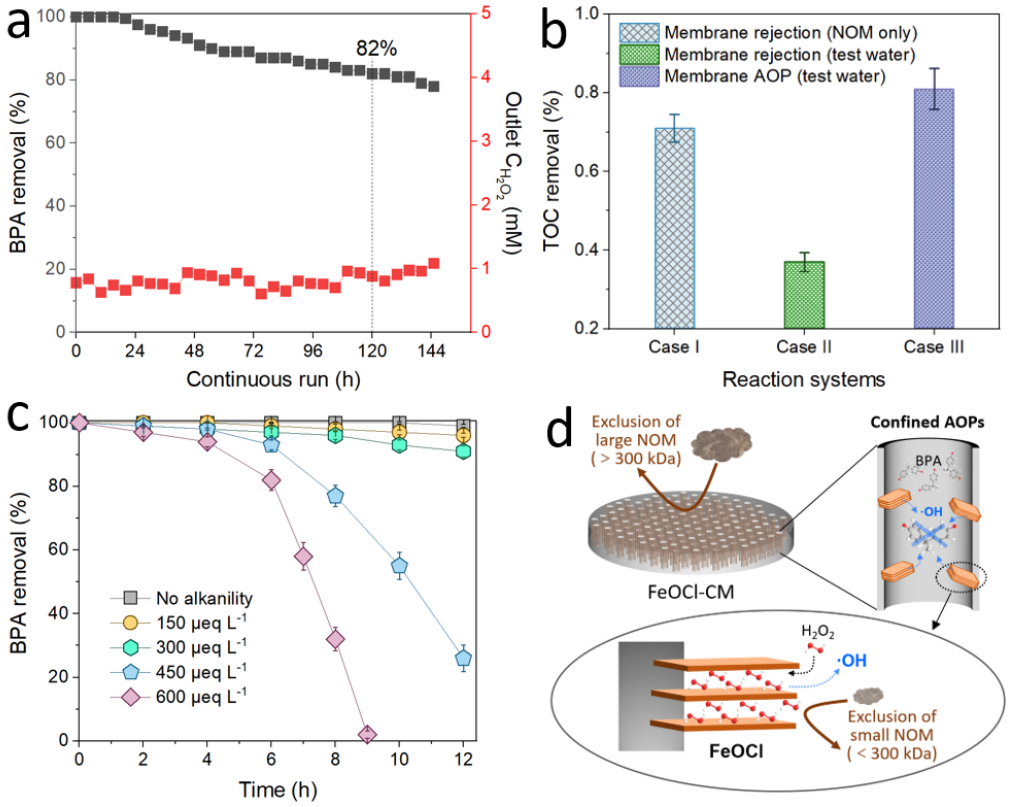

Figure 6. (a) Removal of BPA during a long-term operation of membrane AOPs. Conditions: BPA, 20 μM; H_2O_2, 2 mM; solution pH, 6.2; water flux: 25 LMH. (b) Removal of TOC from the simulated surface water with (test water) and without (NOM only) model pollutants. (c) Membrane AOPs induced removal of BPA under simulated surface water with different background alkalinity (adjusted by $NaHCO_3$). Conditions: BPA, 20 μM; NOM, 5 mg L^{-1} (Suwannee River NOM); the recipe of inorganic constituents referred to the NEWT test water (Nanotechnology Enabled Water Treatment, Table S2 for details); H_2O_2, 2 mM; solution pH, 6.2; water flux: 25 LMH. (d) Schematic diagram of the double size exclusion effect played by the UF membrane reactor (for selective use of •OH) and the layered FeOCl catalyst (for entrance of H_2O_2 to produce •OH).

Performance with Real Water Sample. We further tested FeOCl-CM to treat a water sample collected from a drinking water treatment plant in New Haven, Connecticut and spiked with 20 μM BPA. The tested water was the sand filter effluent with pH = 6.5, alkalinity = 270 μeq L^{-1}, TOC = 1.6 mg L^{-1}, UV 254 nm absorption = 0.017 cm^{-1}, and turbidity = 0.064 NTU. FeOCl-CM completely removed BPA for the first 10 hours of continuous filtration, while the efficiency gradually decreased for the next 10 hours, reaching approximately 82% removal after 20 hours of operation (Figure 7). Considering the relatively high alkalinity of the test water, this result is consistent with the results we obtained with synthetic surface water (Figure 6c).

As discussed above, this gradual loss of performance is likely related to the loss of Fe centers bound to Cl, the preferred site for H_2O_2 binding and activation, due to water coordination and alkaline passivation. We found that the FeOCl-CM reactivity could be effectively recovered by a successive soaking in HCl solution (0.5 M) and annealing treatment (220 °C, 1 hour) for repeated use (Figure 7). This regeneration treatment led to an effective chloride intercalation and restoration of Fe-Cl bonds, through which the crystalline structure of FeOCl was recovered (Figure S13a). High temperature annealing was found to be critical to recover Fe-Cl sites, as evidenced by the ineffective catalyst regeneration with acid-only treatment (Figure S13b). This result again highlights the significance of the Fe-Cl sites that contribute to the overall kinetics of H_2O_2 activation and •OH production. Acid treatment has additional benefits such as chemical removal of deposits, scales, and biofoulants from membrane surfaces. The high temperature treatment, however, cannot be performed online and is impractical, requiring further research of an alternative regeneration technique. Additional study can attempt modulation of the coordination environment of Fe centers by doping isomorphic species such as copper[49] and sulfur[50] that can enhance the adaptability to alkaline conditions.

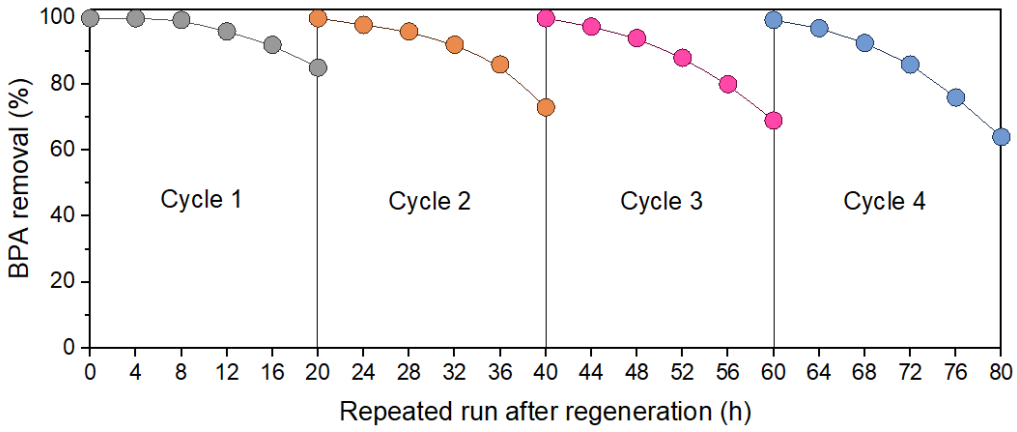

Figure 7. Decontamination of real water. Conditions: BPA, 20 μM; H_2O_2, 2 mM; water flux, 25 LMH. Water samples were collected every four hours and immediately sent to analysis.

In summary, we designed a UF membrane reactor with confined FeOCl nanocatalysts, which exhibited highly efficient catalytic Fenton degradation of organic pollutants under realistic conditions—complex water scenarios with NOM, circumneutral pH, and common UF water fluxes. Unique advantages were featured by the reactions confined within the membrane structure (~ 20 nm pore size): (i) 'selective' AOPs toward organic pollutants due to the size exclusion of larger NOM (> 300 kDa) that effectively avoided the radical quenching, and (ii) enhanced kinetics

of AOPs due to the spatial nanoconfinement effect that augments •OH exposure. Furthermore, the long-term efficient membrane reaction was revealed and can be attributed to both the surface chemistry of FeOCl as well as its layered structure that excludes smaller NOM (< 300 kDa) that entered membrane pores, thus avoiding an invasion of the active sites. With regard to the excellent membrane resiliency to representative complex water matrices, our future work would focus on enhancing the applicability of such reactive membranes for scaled-up treatment scenarios, including the optimization of operating parameters like catalyst/H_2O_2 dosing, the control of in-pore head loss by modulating the growth of nanocatalysts, as well as the aforementioned enhancement of durability to the background water alkalinity.

■ ASSOCIATED CONTENT

Supporting Information

Greater detail of complementary experiments, methods, calculation, and discussion.

■ AUTHOR INFORMATION

Corresponding Author

Jae-Hong Kim − Department of Chemical and Environmental Engineering, Yale University, New Haven, Connecticut 06511, United States; orcid.org/0000-0003-2224-3516; Phone: +1 (203) 432-4386; Email: jaehong.kim@yale.edu

Authors

Shuo Zhang − Department of Chemical and Environmental Engineering, Yale University, New Haven, Connecticut 06511, United States; orcid.org/0000-0002-8663-8616

Tayler Hedtke − Department of Chemical and Environmental Engineering, Yale University, New Haven, Connecticut 06511, United States

Qianhong Zhu − Department of Chemical and Environmental Engineering, Yale University, New Haven, Connecticut 06511, United States

Meng Sun − Department of Chemical and Environmental Engineering, Yale University, New Haven, Connecticut 06511, United States; orcid.org/0000-0002-8188- 9264

Seunghyun Weon − Department of Chemical and Environmental Engineering, Yale University, New Haven, Connecticut 06511, United States; School of Health and Environmental Science, Korea University, Seoul 02841, Republic of Korea; orcid.org/0000-0003-4529-8069

Yumeng Zhao – Department of Chemical and Environmental Engineering, Yale University, New Haven, Connecticut 06511, United States; State Key Laboratory of Urban Water Resource and Environment, Harbin Institute of Technology, Harbin 150090, China

Eli Stavitski – National Synchrotron Light Source II, Brookhaven National Laboratory, Upton, New York 11973, United States

Menachem Elimelech − Department of Chemical and Environmental Engineering, Yale University, New Haven, Connecticut 06511, United States; orcid.org/0000-0003- 4186-1563

Notes

The authors declare no competing financial interests.

■ ACKNOWLEDGMENT

This study was funded by the National Science Foundation Nanosystems Engineering Research Center for Nanotechnology-Enabled Water Treatment (EEC-1449500). This research used beamline 8-ID, Inner Shell Spectroscopy, of the National Synchrotron Light Source II, a U.S. Department of Energy (DOE) Office of Science User Facility operated for the DOE Office of Science by Brookhaven National Laboratory under Contract No. DE-SC0012704.

■ REFERENCES

(1) Tian, Z. Y.; Peter, K. T.; Gipe, A. D.; Zhao, H. Q.; Hou, F.; Wark, D. A.; Khangaonkar, T.; Kolodziej, E. P.; James, C. A. Suspect and Nontarget Screening for Contaminants of Emerging Concern in an Urban Estuary. *Environ. Sci. Technol.* **2020,** *54*, 889-901.

(2) Weiss, J.; Humphrey, C. W. Reaction between Hydrogen Peroxide and Iron Salts. *Nature* **1949,** *163*, 690-691.

(3) Laverne, J. A. The Production of OH Radicals in the Radiolysis of Water with ^{4}He Ions. *Radiat. Res.* **1989,** *118*, 201-210.

(4) Zhang, J.; Nosaka, Y. Mechanism of the OH Radical Generation in Photocatalysis with TiO_2 of Different Crystalline Types. *J. Phys. Chem. C* **2014,** *118*, 10824-10832.

(5) Zhang, S.; Quan, X.; Wang, D. Zhang, S.; Quan, X.; Wang, D. Fluorescence Microscopy Image-Analysis (FMI) for the Characterization of Interphase $HO^{\bullet}$ Production Originated by Heterogeneous Catalysis. *Chem. Commun.* **2017,** *53*, 2575-2577.

(6) Rodrigues, A.; Brito, A.; Janknecht, P.; Proenca, M. F.; Nogueira, R. Quantification of Humic Acids in Surface Water: Effects of Divalent Cations, pH, and Filtration. *J. Environ. Monitor.* **2009,** *11*, 377-382.

(7) Lindsey, M. E.; Tarr, M. A. Inhibition of Hydroxyl Radical Reaction with Aromatics by Dissolved Natural Organic Matter. *Environ. Sci. Technol.* **2000,** *34*, 444-449.

(8) Brame, J.; Long, M. C.; Li, Q. L.; Alvarez, P. Inhibitory Effect of Natural Organic Matter or Other Background Constituents on Photocatalytic Advanced Oxidation Processes: Mechanistic Model Development and Validation. *Water Res.* **2015,** *84*, 362-371.

(9) Wang, T.; Wang, Z. Y.; Wang, P. L.; Tang, Y. Y. An Integration of Photo-Fenton and Membrane Process for Water Treatment by a PVDF@$CuFe_2O_4$ Catalytic Membrane. *J. Membrane Sci.* **2019,** *572*, 419-427.

(10) Wang, X. X.; Sun, M.; Zhao, Y. M.; Wang, C.; Ma, W.; Wong, M. S.; Elimelech, M. In Situ Electrochemical Generation of Reactive Chlorine Species for Efficient Ultrafiltration Membrane Self-Cleaning. *Environ. Sci. Technol.* **2020,** *54*, 6997-7007.
(11) Alpatova, A.; Meshref, M.; McPhedran, K. N.; El-Din, M. G. Composite polyvinylidene fluoride (PVDF) membrane impregnated with Fe_2O_3 nanoparticles and multiwalled carbon nanotubes for catalytic degradation of organic contaminants. *J Membrane Sci* **2015,** *490*, 227-235.
(12) Zheng, J. J.; Wang, Z. W.; Ma, J. X.; Xu, S. P.; Wu, Z. C. Development of an Electrochemical Ceramic Membrane Filtration System for Efficient Contaminant Removal from Waters. *Environ. Sci. Technol.* **2018,** *52*, 4117-4126.
(13) Sun, M.; Zucker, I.; Davenport, D. M.; Zhou, X. C.; Qu, J. H.; Elimelech, M. Reactive, Self-Cleaning Ultrafiltration Membrane Functionalized with Iron Oxychloride Nanocatalysts. *Environ. Sci. Technol.* **2018,** *52*, 8674-8683.
(14) Plakas, K. V.; Mantza, A.; Sklari, S. D.; Zaspalis, V. T.; Karabelas, A. J. Heterogeneous Fenton-like Oxidation of Pharmaceutical Diclofenac by a Catalytic Iron-Oxide Ceramic Microfiltration Membrane. *Chem. Eng. J.* **2019,** *373*, 700-708.
(15) Cui, L. L.; Ding, P. P.; Zhou, M.; Jing, W. H. Energy Efficiency Improvement on in Situ Generating H_2O_2 in a Double-Compartment Ceramic Membrane Flow Reactor Using Cerium Oxide Modified Graphite Felt Cathode. *Chem. Eng. J.* **2017,** *330*, 1316-1325.
(16) Zhang, G. K.; Gao, Y. Y.; Zhang, Y. L.; Guo, Y. D. Fe_2O_3-Pillared Rectorite as an Efficient and Stable Fenton-like Heterogeneous Catalyst for Photodegradation of Organic Contaminants. *Environ. Sci. Technol.* **2010,** *44*, 6384-6389.
(17) Ardo, S. G.; Nelieu, S.; Ona-Nguema, G.; Delarue, G.; Brest, J.; Pironin, E.; Morin, G. Oxidative Degradation of Nalidixic Acid by Nano-magnetite via Fe^{2+}/O_2-Mediated Reactions. *Environ. Sci. Technol.* **2015,** *49*, 4506-4514.
(18) Qian, X. F.; Ren, M.; Zhu, Y.; Yue, D. T.; Han, Y.; Jia, J. P.; Zhao, Y. X. Visible Light Assisted Heterogeneous Fenton-like Degradation of Organic Pollutant via alpha-FeOOH/Mesoporous Carbon Composites. *Environ. Sci. Technol.* **2017,** *51*, 3993-4000.
(19) Feng, C. H.; Li, F. B.; Mai, H. J.; Li, X. Z. Bio-Electro-Fenton Process Driven by Microbial Fuel Cell for Wastewater Treatment. *Environ. Sci. Technol.* **2010,** *44*, 1875-1880.
(20) Acisli, O.; Khataee, A.; Soltani, R. D. C.; Karaca, S. Ultrasound-Assisted Fenton Process Using Siderite Nanoparticles Prepared via Planetary Ball Milling for Removal of Reactive Yellow 81 in Aqueous Phase. *Ultrason. Sonochem.* **2017,** *35*, 210-218.
(21) Fontecha-Camara, M. A.; Moreno-Castilla, C.; Lopez-Ramon, M. V.; Alvarez, M. A. Mixed Iron Oxides as Fenton Catalysts for Gallic Acid Removal from Aqueous Solutions. *Appl. Catal. B-Environ.* **2016,** *196*, 207-215.
(22) Yang, X. J.; Xu, X. M.; Xu, J.; Han, Y. F. Iron Oxychloride (FeOCl): An Efficient Fenton-like Catalyst for Producing Hydroxyl Radicals in Degradation of Organic Contaminants. *J. Am. Chem. Soc.* **2013,** *135*, 16058-16061.
(23) Buxton, G. V.; Greenstock, C. L.; Helman, W. P.; Ross, A. B. Critical Review of Rate Constants for Reactions of Hydrated Electrons, Hydrogen Atoms and Hydroxyl Radicals ($^{\bullet}OH/^{\bullet}O^-$) in Aqueous Solution. *J. Phys. Chem. Ref. Data* **1988,** *17*, 513-886.
(24) Sun, M.; Chu, C.; Geng, F.; Lu, X.; Qu, J.; Crittenden, J.; Elimelech, M.; Kim, J. H. Reinventing Fenton Chemistry: Iron Oxychloride Nanosheet for pH-Insensitive H_2O_2 Activation. *Environ. Sci. Technol. Lett.* **2018,** *5*, 186-191.

(25) Xing, M. Y.; Xu, W. J.; Dong, C. C.; Bai, Y. C.; Zeng, J. B.; Zhou, Y.; Zhang, J. L.; Yin, Y. D. Metal Sulfides as Excellent Co-catalysts for H2O2 Decomposition in Advanced Oxidation Processes. *Chem-Us* **2018**, *4*, 1359-1372.
(26) Jiang, W. L.; Xia, X.; Han, J. L.; Ding, Y. C.; Haider, M. R.; Wang, A. J. Graphene Modified Electro-Fenton Catalytic Membrane for in Situ Degradation of Antibiotic Florfenicol. *Environ. Sci. Technol.* **2018,** *52*, 9972-9982.
(27) Zubir, N. A.; Yacou, C.; Motuzas, J.; Zhang, X. W.; Zhao, X. S.; da Costa, J. C. D. The Sacrificial Role of Graphene Oxide in Stabilising a Fenton-like Catalyst GO-Fe_3O_4. *Chem. Commun.* **2015,** *51*, 9291-9293.
(28) Ji, X. X.; Wang, H. F.; Hu, P. J. First Principles Study of Fenton Reaction Catalyzed by FeOCl: Reaction Mechanism and Location of Active Site. *Rare Metals* **2019,** *38*, 783-792.
(29) Feng, J.; Hu, X. J.; Yue, P. L. Novel Bentonite Clay-Based Fe-Nanocomposite as A Heterogeneous Catalyst for Photo-Fenton Discoloration and Mineralization of Orange II. *Environ. Sci. Technol.* **2004,** *38*, 269-275.
(30) Ren, Y.; Shi, M. Q.; Zhang, W. M.; Dionysiou, D. D.; Lu, J. H.; Shan, C.; Zhang, Y. Y.; Lv, L.; Pan, B. C. Enhancing the Fenton-like Catalytic Activity of nFe_2O_3 by MIL-53(Cu) Support: A Mechanistic Investigation. *Environ. Sci. Technol.* **2020,** *54*, 5258-5267.
(31) Jarrige, I.; Cai, Y. Q.; Shieh, S. R.; Ishii, H.; Hiraoka, N.; Karna, S.; Li, W. H. Charge Transfer in FeOCl Intercalation Compounds and Its Pressure Dependence: An X-Ray Spectroscopic Study. *Phys. Rev. B* **2010,** *82*, 165121.
(32) Yu, T. T.; Li, Q.; Zhao, X. Y.; Xia, H.; Ma, L. Q.; Wang, J. L.; Meng, Y. S.; Shen, X. D. Nanoconfined Iron Oxychloride Material as a High-Performance Cathode for Rechargeable Chloride Ion Batteries. *Acs Energy Lett.* **2017,** *2*, 2341-2348.
(33) Karimnezhad, H.; Navarchian, A. H.; Gheinani, T. T.; Zinadini, S. Amoxicillin Removal by Fe-Based Nanoparticles Immobilized on Polyacrylonitrile Membrane: Individual Nanofiltration or Fenton Reaction, vs. Engineered Combined Process. *Chem. Eng. Res. Des.* **2020,** *153*, 187-200.
(34) Zhang, L. P.; Liu, Z.; Faraj, Y.; Zhao, Y.; Zhuang, R.; Xie, R.; Ju, X. J.; Wang, W.; Chu, L. Y. High-Flux Efficient Catalytic Membranes Incorporated with Iron-Based Fenton-like Catalysts for Degradation of Organic Pollutants. *J. Membrane Sci.* **2019,** *573*, 493-503.
(35) Zhang, Y. J.; Yuan, M. Y.; Lin, R.; Ma, J. Degradation of Orange IV Solution by a Fenton-like Process Using Fe^{3+}/PVDF-PMMA Catalytic Membrane. *J. Environ. Eng.* **2014,** *140*, 06014001.
(36) Lan, H. C.; Wang, F.; Lan, M.; An, X. Q.; Liu, H. J.; Qu, J. H. Hydrogen-Bond-Mediated Self-Assembly of Carbon-Nitride-Based Photo-Fenton-like Membranes for Wastewater Treatment. *Environ. Sci. Technol.* **2019,** *53*, 6981-6988.
(37) Finkelstein, E.; Rosen, G. M.; Rauckman, E. J. Spin Trapping. Kinetics of the Reaction of Superoxide and Hydroxyl Radicals with Nitrones. *J. Am. Chem. Soc.* **1980,** *102*, 4994-4999.
(38) Carbajo, J.; Tolosana-Moranchel, A.; Casas, J. A.; Faraldos, M.; Bahamonde, A. Analysis of Photoefficiency in TiO_2 Aqueous Suspensions: Effect of Titania Hydrodynamic Particle Size and Catalyst Loading on Their Optical Properties. *Appl. Catal. B-Environ.* **2018,** *221*, 1-8.
(39) Zhang, S.; Sun, M.; Hedtke, T.; Deshmukh, A.; Zhou, X.; Weon, S.; Elimelech, M.; Kim, J. H. Mechanism of Heterogeneous Fenton Reaction Kinetics Enhancement under Nanoscale Spatial Confinement. *Environ. Sci. Technol.* **2020,** *54*, 10868-10875.
(40) Peretz, J.; Vrooman, L.; Ricke, W. A.; Hunt, P. A.; Ehrlich, S.; Hauser, R.; Padmanabhan, V.; Taylor, H. S.; Swan, S. H.; VandeVoort, C. A.; Flaws, J. A. Bisphenol A and Reproductive

Health: Update of Experimental and Human Evidence, 2007-2013. *Environ. Health Persp.* **2014,** *122*, 775-786.
(41) Inadera, H. Neurological Effects of Bisphenol A and Its Analogues. *Int. J. Med. Sci.* **2015,** *12*, 926-936.
(42) Long, M. C.; Brame, J.; Qin, F.; Bao, J. M.; Li, Q. L.; Alvarez, P. J. J. Phosphate Changes Effect of Humic Acids on TiO_2 Photocatalysis: From Inhibition to Mitigation of Electron-Hole Recombination. *Environ. Sci. Technol.* **2017,** *51*, 514-521.
(43) Zhao, Y. H.; Abraham, M. H.; Zissimos, A. M. Fast Calculation of van der Waals Volume as A Sum of Atomic and Bond Contributions and Its Application to Drug Compounds. *J. Org. Chem.* **2003,** *68*, 7368-7373.
(44) Herber, R. H.; Cassell, R. A. Synthesis, Hyperfine Interactions, and Lattice Dynamics of the Intercalation Compound FeOCl(Kryptofix-21)$_{1/18}$. *Inorg. Chem.* **1982,** *21*, 3713-3716.
(45) Yang, X. J.; Tian, P. F.; Zhang, X. M.; Yu, X.; Wu, T.; Xu, J.; Han, Y. F. The Generation of Hydroxyl Radicals by Hydrogen Peroxide Decomposition on FeOCl/SBA-15 Catalysts for Phenol Degradation. *AICHE J.* **2015,** *61*, 166-176.
(46) Gu, Y. W.; Gong, L.; Qi, J. L.; Cai, S. C.; Tu, W. X.; He, F. Sulfidation Mitigates the Passivation of Zero Valent Iron at Alkaline pHs: Experimental Evidences and Mechanism. *Water Res.* **2019,** *159*, 233-241.
(47) Alowitz, M. J.; Scherer, M. M. Kinetics of Nitrate, Nitrite, and Cr(VI) Reduction by Iron Metal. *Environ. Sci. Technol.* **2002,** *36*, 299-306.
(48) Omernik, J. M.; Griffith, G. E. Total Alkalinity of Surface Waters: A Map of the Upper Midwest Region of the United-States. *Environ. Manage.* **1986,** *10*, 829-839.
(49) Jin, H.; Tian, X. K.; Nie, Y. L.; Zhou, Z. X.; Yang, C.; Li, Y.; Lu, L. Q. Oxygen Vacancy Promoted Heterogeneous Fenton-like Degradation of Ofloxacin at pH 3.2-9.0 by Cu Substituted Magnetic Fe_3O_4@FeOOH Nanocomposite. *Environ. Sci. Technol.* **2017,** *51*, 12699-12706.
(50) Du, J. K.; Bao, J. G.; Fu, X. Y.; Lu, C. H.; Kim, S. H. Mesoporous Sulfur-Modified Iron Oxide as an Effective Fenton-like Catalyst for Degradation of Bisphenol A. *Appl. Catal. B-Environ.* **2016,** *184*, 132-141.

621 **TOC Graphic**

622